Chemical Science

ROYAL SOCIETY OF CHEMISTRY

EDGE ARTICLE

View Article Online
View Journal | View Issue

Cite this: *Chem. Sci.*, 2023, **14**, 1551

All publication charges for this article have been paid for by the Royal Society of Chemistry

Isomeric thermally activated delayed fluorescence emitters for highly efficient organic light-emitting diodes†

Yanyan Liu,‡[a] Jiaji Yang,‡[b] Zhu Mao,*[c] Yuyuan Wang,[a] Juan Zhao,*[d] Shi-Jian Su*[b] and Zhenguo Chi*[a]

Received 17th November 2022
Accepted 12th January 2023

DOI: 10.1039/d2sc06335b

rsc.li/chemical-science

The isomeric strategy is an important design concept in molecular design that has a non-negligible influence on molecular properties. Herein, two isomeric thermally activated delayed fluorescence (TADF) emitters (**NTPZ** and **TNPZ**) are constructed with the same skeleton consisting of an electron donor and electron acceptor but different connection sites. Systematic investigations show that **NTPZ** exhibits a small energy gap, large up-conversion efficiency, low non-radiative decay, and high photoluminescence quantum yield. Further theoretical simulations reveal that the excited molecular vibrations play a key role in regulating the non-radiative decays of the isomers. Therefore, an **NTPZ** based OLED achieves better electroluminescence performances, such as a higher external quantum efficiency of 27.5% compared to a **TNPZ** based OLED (18.3%). This isomeric strategy not only provides an opportunity to deeply understand the relationship between substituent locations and molecular properties, but also affords a simple and effective strategy to enrich TADF materials.

Introduction

Pure organic thermally activated delayed fluorescence (TADF) emitters have attracted much attention for applications in organic light-emitting diodes (OLEDs) due to their advantages of 100% internal quantum efficiency *via* the reverse intersystem crossing (RISC) process from the triplet (T_1) state to the singlet (S_1) state.[1–3] To achieve an efficient RISC process, the general molecule design strategy is to construct a twisted connection between the electron donor (D) and electron acceptor (A) with a D–π–A skeleton, which can separate the highest occupied molecular orbital (HOMO) and the lowest unoccupied molecular orbital (LUMO) to reduce the S_1–T_1 energy gap (ΔE_{ST}) so as to enhance RISC up-conversion.[4,5] However, the isolated HOMO–LUMO tends to decrease radiative decay with a low quantum efficiency.[6] Additionally, for highly efficient TADF emitters, low non-radiative decays are also required simultaneously.[7] To solve this dilemma, several design strategies have been proposed, such as intensifying intramolecular charge transfer (ICT),[8–10] increasing molecular rigidity,[11–13] and incorporating through-space charge transfer.[14–16] Among these strategies, the twisted angles between the donor and acceptor should be carefully modulated as should their electron-donating and electron-withdrawing abilities.[17] Therefore, it is essential to gain a deep understanding of the properties of the selected moieties (D or A) to realize high-efficiency TADF molecules, revealing the difficulty of molecular design.

As known, structural isomers are different compounds that have the same molecular formula but the atoms are attached in distinct ways by covalent bonds, which have significant effects on chemical and physical properties.[18,19] Isomers with different structures can induce geometric and electronic structure changes in molecules.[20] In the past decade, much attention has been paid to the development of new types of electron donors and acceptors to construct highly efficient TADF molecules.[21,22] In contrast, applying the same donor and acceptor to construct TADF molecules has rarely been considered. Taking this into account, isomers with the TADF feature can be accomplished by manipulating different substitution positions of the same electron donor/acceptor to regulate excited states and thus modulate photophysical processes.[23] Therefore, further studies on the structure–property relationship of different isomers are of great significance to the design of TADF molecules.

[a]*PCFM Lab, GDHPPC Lab, Guangdong Engineering Technology Research Center for High-performance Organic and Polymer Photoelectric Functional Films, State Key Laboratory of OEMT, School of Chemistry, Sun Yat-sen University, Guangzhou 510275, China. E-mail: chizhg@mail.sysu.edu.cn*

[b]*State Key Laboratory of Luminescent Materials and Devices, Institute of Polymer Optoelectronic Materials and Devices, South China University of Technology, Guangzhou 510640, China. E-mail: mssjsu@scut.edu.cn*

[c]*Shenzhen Institute of Advanced Electronic Materials, Shenzhen Institutes of Advanced Technology, Chinese Academy of Sciences, Shenzhen 518055, China. E-mail: maozhu1989@hotmail.com*

[d]*School of Materials Science and Engineering, Sun Yat-sen University, Guangzhou 510275, China. E-mail: zhaoj95@mail.sysu.edu.cn*

† Electronic supplementary information (ESI) available. See DOI: https://doi.org/10.1039/d2sc06335b

‡ Contributed equally.

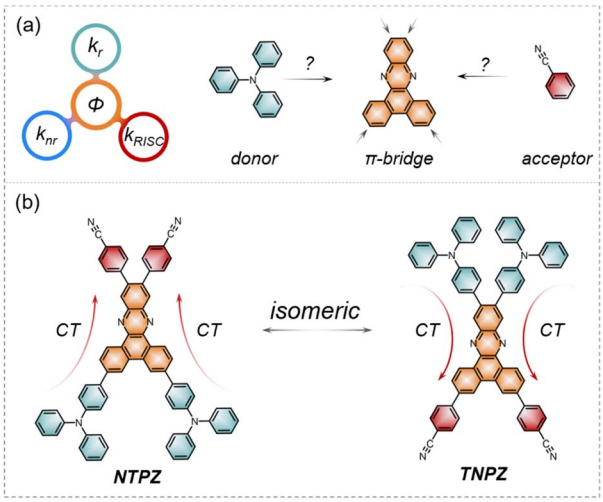

Fig. 1 (a) Key parameters and the moieties of typical TADF molecules and (b) chemical structures of NTPZ and TNPZ in this work.

With this hypothesis, two isomeric TADF emitters based on a dibenzo[*a*,*c*]phenazine (PZ) skeleton, namely 4,4′-(3,6-bis(4-(diphenylamino)phenyl)dibenzo[*a*,*c*]-phenazine-11,12-diyl)dibenzonitrile (**NTPZ**) and 4,4′-(11,12-bis(4-(diphenylamino)phenyl)-dibenzo[*a*,*c*]phenazine-3,6-diyl)-dibenzonitrile (**TNPZ**) with the same donor and acceptor units but different connection locations were designed and synthesized (Fig. 1b). PZ was selected as the backbone considering its large conjugate plane, excellent thermal stability, and easy structural modification, while triphenylamine was chosen considering its strong electron donor ability and high hole mobility.[24] **NTPZ** and **TNPZ** have similar photophysical properties due to their identical components, while **NTPZ** exhibits a significantly faster RISC process and lower non-radiative decay than **TNPZ**, thereby promoting electroluminescence performance. Further experimental and theoretical analyses demonstrate that the isomers exhibit different excited structural relaxations, resulting in varied efficiencies. The results give us an opportunity to get a deep understanding of the relationship between substituent positions and molecular properties. Meanwhile, the isomeric strategy of exchanging donor and acceptor positions enriches the structural diversity of TADF molecules. Therefore, this work provides an effective new strategy for the development of efficient TADF emitters.

Results and discussion

Theoretical calculations

The synthetic procedures are shown in Scheme S1† (ESI) and structural characterization studies are conducted by proton nuclear magnetic resonance spectroscopy, carbon nuclear magnetic resonance spectroscopy and high resolution mass spectroscopy (Fig. S1–S9†). Density functional theory calculations of **NTPZ** and **TNPZ** were first carried out using the B3LYP/6-311G(*) level to optimize molecular geometries. The frontier molecule orbital distributions of **NTPZ** and **TNPZ** are calculated and delineated as shown in Fig. 2, showing that the HOMOs are

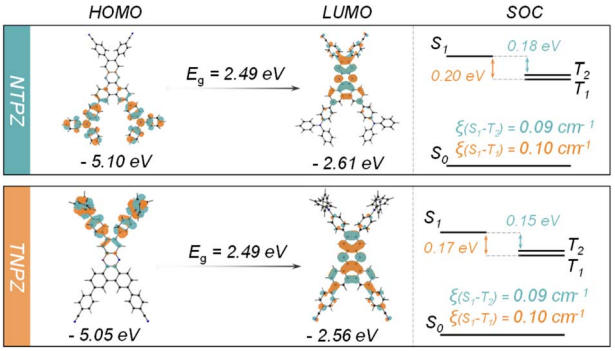

Fig. 2 Theoretical calculations of NTPZ and TNPZ based on gas states.

mainly distributed on the TPA group and the LUMOs are located on the PZ core while extending to the benzene cyano unit. Such thorough separation of the HOMO–LUMO drives the reduction in ΔE_{ST} (0.20 eV and 0.17 eV for **NTPZ** and **TNPZ**, respectively), which is beneficial for an efficient RISC process. Natural transition orbital (NTO) and spin-orbital coupling matrix (SOC) investigations are performed to further evaluate excited state characteristics using time-dependent density functional theory. As displayed in Fig. S10 and S11,† the ground state $S_0 \rightarrow S_1$ transition represents the charge transfer (CT) transition from the TPA donor to the PZ acceptor. Intriguingly, the lower-lying triplet states (T_1 and T_2) of the two isomers show hybrid charge transfer and locally excited (LE) features, which are crucial to enhance the RISC process *via* non-adiabatic coupling.[25] These results indicate that the two molecules constructed by the same units exhibit the potential to act as TADF materials. Intriguingly, the theoretical results reveal that the two isomers with different substitution positions show analogous electronic features of excited states, which is different from previously reported cases.[26,27]

Photophysical properties

Ultraviolet-visible (UV-vis) absorption and photoluminescence (PL) spectra of **NTPZ** and **TNPZ** in dilute toluene solutions at room temperature were measured to explore the effect of different connection modes on photophysical properties. As presented in Fig. 3a, the two molecules show similar absorption features due to their identical components. The high energy absorption peaks before 409 nm can be assigned to the intramolecular LE transitions and the low energy absorption peaks (410–550 nm) should be attributed to the intramolecular charge transfer (ICT) transitions from the donor to the acceptor. Besides, **NTPZ** and **TNPZ** also show similar PL emission peaks that are located at 557 and 563 nm, respectively. Both compounds show broad and structureless emissions, suggesting their ICT characteristics, which can be further proved by the solvatochromic effect (Fig. S12 and S13†). It can be seen that the absorption peaks of **NTPZ** or **TNPZ** are very similar while the emission peaks show an apparently bathochromic shift with the solvent polarity increasing from non-polar hexane to polar trichloromethane, indicating the ICT characters of these molecules. Moreover, the transient PL decay spectra of **NTPZ** and **TNPZ** were recorded in toluene solutions (Fig. 3c), which exhibit single exponential prompt decays with

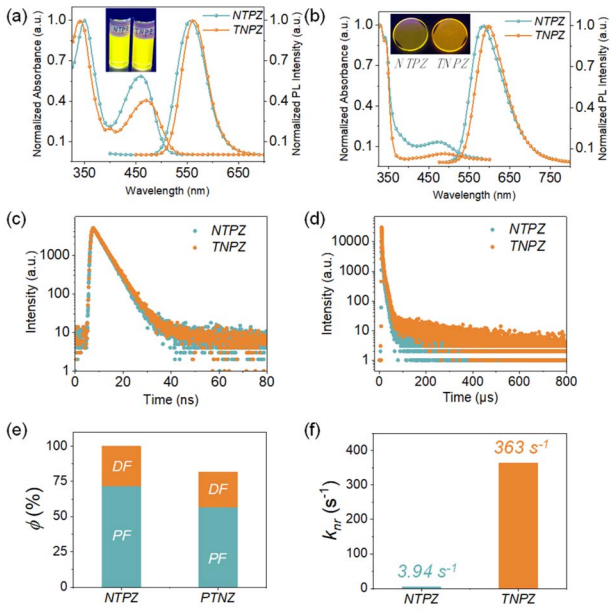

Fig. 3 UV-vis absorption and PL spectra in (a) toluene solutions and (b) 10 wt% doped CBP films (inset: images of toluene solution and 10 wt% doped CBP films of emitters under a UV lamp, excitation wavelength: 365 nm), transient PL decay curves in (c) toluene solutions and (d) 10 wt% doped CBP films for **NTPZ** and **TNPZ**, and (e) PLQY and (f) non-radiative rate of the isomers in doped films.

a fluorescence lifetime of 4.1 and 4.3 ns, respectively. The slightly longer lifetime of **TNPZ** indicates the stronger ICT effect, which is consistent with the UV-vis absorption and PL spectra. Additionally, the ΔE_{ST} values of **NTPZ** and **TNPZ** were calculated from the edges of fluorescence spectra at room temperature and phosphorescence spectra at 77 K (Fig. S14 and S15†), which are 0.20 and 0.22 eV in toluene solutions and 0.10 and 0.19 eV in 10 wt% doped CBP films, respectively, suggesting the possibility of an up-conversion process. It should be noted that the different ΔE_{ST} values between the theoretical and experimental results can be assigned to external environment reorganization effects.[28]

In a further set of experiments, the doped films of a 10 wt% emitter in a 4,4′-bis(9*H*-carbazol-9-yl)biphenyl (CBP) host were investigated. Similar to the toluene solutions, the two films exhibit similar absorption and emission features that originate from the same component. As shown in Fig. 3b, the broad absorption at around 400–450 nm can be assigned to the ICT features of the two isomers, which can also be identified by the structureless emissions of the films with PL peaks at 583 and 588 nm for **NTPZ** and **TNPZ**, respectively. Meanwhile, the transient PL decay spectra were measured on films (Fig. 3d). As expected, the decay curves exhibit biexponential features composed of a nanosecond prompt decay and a microsecond delayed decay, with delayed lifetimes of 71 μs and 125 μs for **NTPZ** and **TNPZ** in film states, respectively. The microsecond lifetime suggests the participation of triplet excitons, which can further be verified by oxygen-sensitive PL spectra, showing increased luminescence intensity under vacuum conditions instead of air conditions (Fig. S16†). Additionally, temperature-dependent transient decay spectra of the molecules from 100 K to 300 K were recorded (Fig. S17†). The proportion of the delayed components shows an increased tendency when increasing temperature from 100 K to 300 K, demonstrating the TADF properties of the two isomeric molecules. In order to reveal more detailed photophysical properties of the isomers, photoluminescence quantum yields (PLQYs) of **NTPZ** and **TNPZ** were measured (Fig. 3e), which reach up to nearly 100% and 82% under oxygen-free conditions, respectively. Thereafter, kinetic parameters are obtained based on the PLQYs and lifetime results (Table 1). Intriguingly, the k_{RISC} constant of **NTPZ** is higher than that of **TNPZ**, while the nonradiative decay rate (k_{nr}) constant of **NTPZ** is significantly reduced by two orders of magnitude (Fig. 3f), implying an excellent TADF feature and efficient exciton utilization for **NTPZ**. The detailed photophysical parameters reveal that the different constitution types of the same donors and acceptor have great influence on the TADF performances of isomer molecules. Notably, the emission wavelength of **TNPZ** presents a bathochromic shift in the monomolecular state (Fig. 3a and b), while it is opposite in the aggregated state (Fig. S18†), ascribed to the way of molecular stacking, which can be proved by powder X-ray diffraction (Fig. S19†).[29,30]

In order to reveal the relationship between excited-stated structural motions and non-radiative pathways, theoretical simulations were further carried out. Generally, excited-molecular vibrations can be restricted by intramolecular interactions to afford a lower non-radiative decay. In this regard, reduced density gradient (RDG) analysis was performed to unveil intramolecular interactions.[31] Due to the steric hindrance of the isomers, plenty of intramolecular interaction regions are found as displayed in Fig. 4a. Intriguingly, the interaction regions exhibit a significant difference in triphenylamine moieties for the two isomers. In a further set of experiments, root-mean-square-deviation (RMSD) calculations are executed to evaluate conformation changes of the

Table 1 Summary of photophysical properties

Comp.	λ_A[a] (nm)	λ_{em}[b] (nm)	PLQY[c] (%)	Φ_{PF}[d] (%)	Φ_{DF}[e] (%)	τ_{PF}[f] (ns)	τ_{DF}[g] (μs)	k_r[h] (s^{-1})	k_{nr}[i] (s^{-1})	k_{ISC}[j] (s^{-1})	k_{RISC}[k] (s^{-1})
NTPZ	473	583	100	72	28	7.0	71	1.03×10^8	3.94×10^0	2.88×10^7	5.48×10^3
TNPZ	489	589	82	57	25	4.3	125	1.32×10^8	3.63×10^2	4.03×10^7	2.86×10^3

[a] Absorption peak in a 10 wt% doped CBP film. [b] PL emission peak in a 10 wt% doped CBP film. [c] Quantum efficiency in a 10 wt% doped CBP film (excitation wavelength: 470 nm). [d] Quantum efficiency of prompt emission. [e] Quantum efficiency of delayed emission. [f] Prompt fluorescence lifetime component (excitation wavelength: 470 nm and emission wavelengths: 583 and 589 nm). [g] Delayed fluorescence lifetime component (excitation wavelength: 470 nm and emission wavelengths: 583 and 589 nm). [h] Rate constant of radiative decay for the singlet excited state. [i] Rate constant of non-radiative decay for the singlet excited state. [j] Rate constant of ISC. [k] Rate constant of RISC.

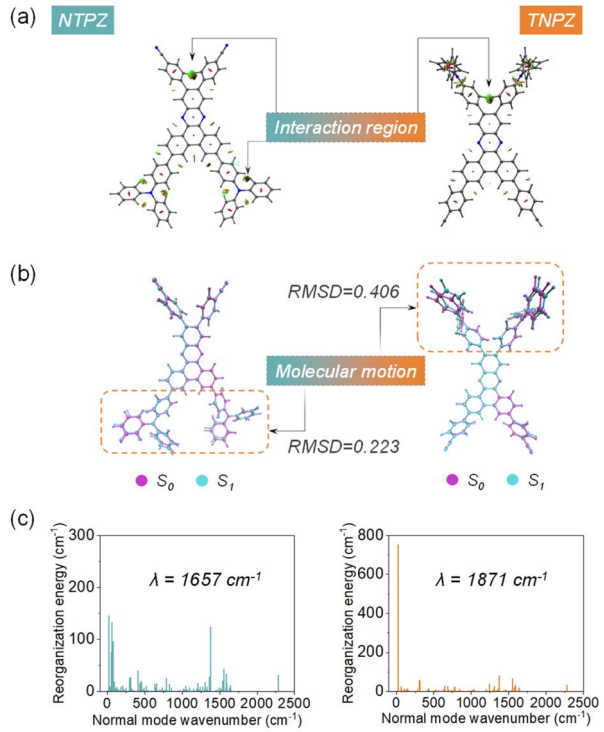

Fig. 4 (a) RDG analysis of the isomers, (b) RMSD of the ground and excited states of the isomers, and (c) reorganization energy analysis of the isomers.

ground state (S_0) and excited singlet state (S_1) based on optimized molecular geometry for these molecules (Fig. 4b). **TNPZ** presents a much higher RMSD value (0.406) than **NTPZ** (0.223); the higher RMSD means larger conformation regulations between S_0 and S_1, thus resulting in more non-radiative transition channels of excited-state molecules.[32]

Meanwhile, reorganization energy (λ) is an indicator of geometry changes in the S_0 state and S_1 state, which also reflects the contribution of intramolecular motions to non-radiative decay.[33] Therefore, to investigate the detailed features of exicited-molecular motions, the λ values *versus* normal mode of **NTPZ** and **TNPZ** were calculated to be 1657 cm^{-1} and 1871 cm^{-1} (Fig. 4c), respectively. As expected, the primarily normal mode (21.59 cm^{-1}) contribution of reorganization in **TNPZ** could be assigned to the vibrations of the triphenylamine moiety (Fig. S20†), which is the main reason for fast non-radiative decay in **TNPZ**. These results demonstrate that the significant molecular vibrations in **TNPZ** are the main reason for the lower quantum efficiency.

Thermal stability

To confirm the high rigidity and excellent thermal stability, thermogravimetric analysis and differential scanning calorimetry were implemented (Fig. S21†), and the decomposition temperatures (T_d: corresponding to 5% weight loss) of **NTPZ** and **TNPZ** are 549 and 600 °C, respectively, while there is no significant glass transition temperature due to the high rigidity. The excellent thermal properties of **NTPZ** and **TNPZ** prove that they are suitable for vacuum deposition techniques to fabricate OLEDs.

Horizontal dipole ratio (HDR)

The HDR orientation of **NTPZ** and **TNPZ** was studied *via* the polarized angle-dependent PL intensity at the maximum emission peak in CBP doped films. As illustrated in Fig. 5a, the HDR orientation is simulated to be 88% and 92% for **NTPZ** and **TNPZ**, respectively, which is higher than 67% for purely isotropic emitters, indicating that the two emitters possess excellent HDRs in the CBP host materials. In addition, the transition dipole moment (TDM) from S_1 to S_0 was calculated based on optimized S_1 state structures (Fig. 5b); the TDM vectors of both emitters represent that the direction of TDM is mainly along the molecular long *x*-axis, especially for **TNPZ**, where the *X* plane and transition dipole moment are elongated despite the distorted conformation, which is beneficial to improve the outcoupling coefficient.[34] These results reveal that **NTPZ** and **TNPZ** have great potential to enhance light harvesting efficiency without any external light out-coupling measurements.

Electroluminescence (EL) performance

To investigate the EL performance of the TADF emitters, multilayer devices with structures of ITO/HATCN (5 nm)/TAPC (30 nm)/mCP (10 nm)/CBP: 10 wt% **NTPZ** or **TNPZ** (20 nm)/B3PYMPM (70 nm)/LiF (1 nm)/Al (150 nm) were constructed. Herein, HATCN is 2,3,6,7,10,11-hexacyano-1,4,5,8,9,12-hexaazatriphenylene, TAPC is 1,1-bis(4-di-*p*-tolylaminophenyl)cyclohexane, mCP is *m*-bis(*N*-carbazolyl)benzene, and CBP is 4,4′-bis(9*H*-carbazol-9-yl)biphenyl. In both devices, HATCN acted as a hole-injection layer; TAPC and B3PYMPM are employed as a hole-transporting layer and an electron-transporting layer, respectively; mCP is used as an exciton blocking layer because its high triplet energy can help prevent energy transfer and loss, thus benefiting high device efficiency.

The OLED device structure and EL performances including current density–voltage–luminance curves, external quantum efficiency (EQE), and EL spectra are illustrated in Fig. 6 and the key device data are summarized in Table S1.† The turn-on

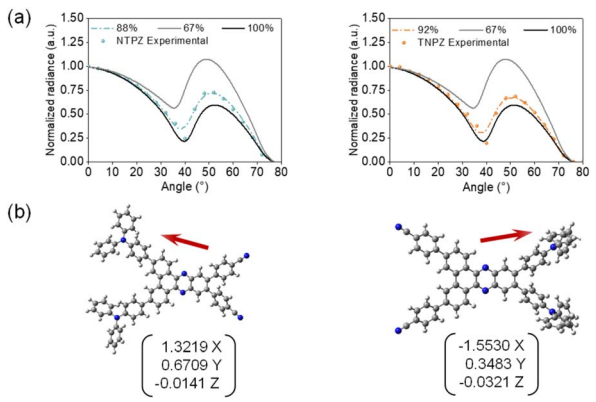

Fig. 5 (a) Measured p-polarized PL intensity at the maximum emission peak in 10 wt% emitter doped CBP films and simulated curves (lines and dotted lines) with different horizontal dipole ratios for NTPZ and TNPZ. (b) The transition dipole moment vectors and the direction of NTPZ and TNPZ.

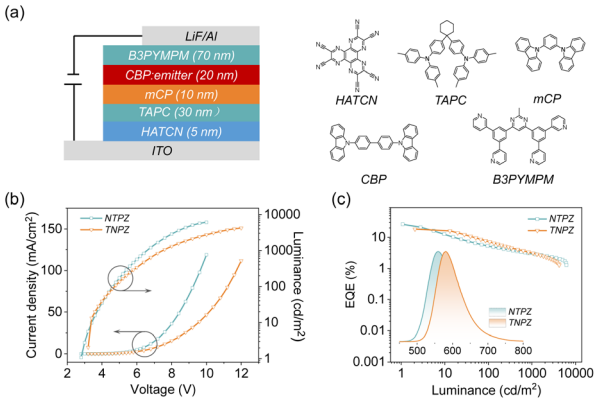

Fig. 6 (a) OLED device structure and molecular structures of the materials. (b) Current density–voltage–luminance curves and (c) EQE–luminance curves and EL spectra (inset) of OLEDs.

voltages (at a brightness of 1 cd m^{-2}) of **NTPZ** and **TNPZ** are 2.8 and 3.2 V, respectively, and the relatively lower turn-on voltage and higher current density of **NTPZ**-OLED suggest a better charge carrier transport characteristic of the **NTPZ**-OLED. Correspondingly, the **NTPZ**-OLED achieves superior EL characteristics with a maximum EQE, current efficiency (CE) and power efficiency (PE) of 27.5%, 82.3 cd A^{-1}, and 92.3 lm W^{-1}, respectively. In comparison, the **TNPZ**-OLED shows a maximum EQE, CE and PE of 18.3%, 50.0 cd A^{-1}, and 49.1 lm W^{-1}, respectively. The outstanding EL performance of the **NTPZ**-OLED device can be attributed to the high PLQY, large k_{RISC} and small k_{nr} of **NTPZ**.

Conclusion

In summary, we propose an isomeric strategy of exchanging donor and acceptor positions to design efficient TADF emitters based on the dibenzo[*a*,*c*]phenazine skeleton, resulting in two isomeric TADF emitters, namely **NTPZ** and **TNPZ** with the same donor and acceptor units but different connection sites. Theoretical and experimental investigations reveal that the distinct connecting location has a significant impact on the molecular properties, including the reverse intersystem crossing process, non-radiative decays, photoluminescence quantum yield and electroluminescence performances. In comparison to the **TNPZ**-OLED, the **NTPZ**-OLED exhibits better EL performances, such as a higher maximum EQE of 27.5%, which are related to the large k_{RISC}, low k_{nr}, and high PLQY of **NTPZ**. This work not only enriches the structural diversity of TADF emitters but also provides an effective new strategy for future development of electroluminescent materials.

Data availability

All the data supporting this article have been provided in the main text and the ESI.†

Author contributions

Y. Liu, J. Yang, and Y. Wang designed and performed the experiments with the help of Z. Mao, J. Zhao, S.-J. Su and Z. Chi. All the authors contributed to the analyses of data. Y. Liu and J. Yang contributed equally to this work.

Conflicts of interest

There are no conflicts to declare.

Acknowledgements

This work was financially supported by the National Natural Science Foundation of China (NSFC: 51733010, 52073316, and 51603232), Basic and Applied Basic Research Foundation of GuangDong Province (202102020951 and 2022B1515020052) and Guangdong Natural Science Funds for Distinguished Young Scholar (2017B030306012). We appreciate Dr Lianrui Hu for help in reorganization energy calculations.

Notes and references

1 Y. Tao, K. Yuan, T. Chen, P. Xu, H. Li, R. Chen, C. Zheng, L. Zhang and W. Huang, *Adv. Mater.*, 2014, **26**, 7931–7958.
2 H. Uoyama, K. Goushi, K. Shizu, H. Nomura and C. Adachi, *Nature*, 2012, **492**, 234–238.
3 G. Hong, X. Gan, C. Leonhardt, Z. Zhang, J. Seibert, J. M. Busch and S. Brase, *Adv. Mater.*, 2021, **33**, 2005630.
4 M. Y. Wong and E. Zysman-Colman, *Adv. Mater.*, 2017, **29**, 1605444.
5 Y. Im, M. Kim, Y. J. Cho, J.-A. Seo, K. S. Yook and J. Y. Lee, *Chem. Mater.*, 2017, **29**, 1946–1963.
6 J. X. Chen, K. Wang, C. J. Zheng, M. Zhang, Y. Z. Shi, S. L. Tao, H. Lin, W. Liu, W. W. Tao, X. M. Ou and X. H. Zhang, *Adv. Sci.*, 2018, **5**, 1800436.
7 Y. Liu, J. Yang, Z. Mao, X. Chen, Z. Yang, X. Ge, X. Peng, J. Zhao, S. J. Su and Z. Chi, *ACS Appl. Mater. Interfaces*, 2022, **14**, 33606–33613.
8 W. Li, B. Li, X. Cai, L. Gan, Z. Xu, W. Li, K. Liu, D. Chen and S. J. Su, *Angew. Chem., Int. Ed.*, 2019, **58**, 11301–11305.
9 Z. Xie, C. Cao, Y. Zou, X. Cao, C. Zhou, J. He, C. S. Lee and C. Yang, *Adv. Funct. Mater.*, 2022, 2112881.
10 D. G. Congrave, B. H. Drummond, P. J. Conaghan, H. Francis, S. T. E. Jones, C. P. Grey, N. C. Greenham, D. Credgington and H. Bronstein, *J. Am. Chem. Soc.*, 2019, **141**, 18390–18394.
11 J. X. Chen, W. W. Tao, W. C. Chen, Y. F. Xiao, K. Wang, C. Cao, J. Yu, S. Li, F. X. Geng, C. Adachi, C. S. Lee and X. H. Zhang, *Angew. Chem., Int. Ed.*, 2019, **58**, 14660–14665.
12 Z. Zhao, Z. Cai, X. Wu, H. Liu, J. Guo, D. Yang, D. Ma and B. Z. Tang, *Angew. Chem., Int. Ed.*, 2021, **60**, 23635–23640.
13 Y. J. Yu, Y. Hu, S. Y. Yang, W. Luo, Y. Yuan, C. C. Peng, J. F. Liu, A. Khan, Z. Q. Jiang and L. S. Liao, *Angew. Chem., Int. Ed.*, 2020, **59**, 21578–21584.

14 T. Huang, Q. Wang, S. Xiao, D. Zhang, Y. Zhang, C. Yin, D. Yang, D. Ma, Z. Wang and L. Duan, *Angew. Chem., Int. Ed.*, 2021, **60**, 23771–23776.
15 C. C. Peng, S. Y. Yang, H. C. Li, G. H. Xie, L. S. Cui, S. N. Zou, C. Poriel, Z. Q. Jiang and L. S. Liao, *Adv. Mater.*, 2020, **32**, 2003885.
16 J. Liu, H. Zhang, L. Hu, J. Wang, J. W. Y. Lam, L. Blancafort and B. Z. Tang, *J. Am. Chem. Soc.*, 2022, **144**, 7901–7910.
17 Y. K. Wang, C. C. Huang, H. Ye, C. Zhong, A. Khan, S. Y. Yang, M. K. Fung, Z. Q. Jiang, C. Adachi and L. S. Liao, *Adv. Opt. Mater.*, 2020, **8**, 1901150.
18 Z. Yang, Z. Mao, Z. Xie, Y. Zhang, S. Liu, J. Zhao, J. Xu, Z. Chi and M. P. Aldred, *Chem. Soc. Rev.*, 2017, **46**, 915–1016.
19 D. Barman, K. Narang, R. Gogoi, D. Barman and P. K. Iyer, *J. Mater. Chem. C*, 2022, **10**, 8536–8583.
20 T. Yang, Z. Cheng, Z. Li, J. Liang, Y. Xu, C. Li and Y. Wang, *Adv. Funct. Mater.*, 2020, **30**, 2002681.
21 B. Zhao, H. Wang, C. Han, P. Ma, Z. Li, P. Chang and H. Xu, *Angew. Chem., Int. Ed.*, 2020, **59**, 19042–19047.
22 J.-X. Chen, W.-W. Tao, Y.-F. Xiao, S. Tian, W.-C. Chen, K. Wang, J. Yu, F.-X. Geng, X.-H. Zhang and C.-S. Lee, *J. Mater. Chem. C*, 2019, **7**, 2898–2904.
23 H. Liu, J. Zeng, J. Guo, H. Nie, Z. Zhao and B. Z. Tang, *Angew. Chem., Int. Ed.*, 2018, **57**, 9290–9294.
24 Y. Liu, J. Yang, Z. Mao, D. Ma, Y. Wang, J. Zhao, S. J. Su and Z. Chi, *Adv. Opt. Mater.*, 2022, 2201695.
25 Z. Yang, Z. Mao, C. Xu, X. Chen, J. Zhao, Z. Yang, Y. Zhang, W. Wu, S. Jiao, Y. Liu, M. P. Aldred and Z. Chi, *Chem. Sci.*, 2019, **10**, 8129–8134.
26 L. S. Cui, H. Nomura, Y. Geng, J. U. Kim, H. Nakanotani and C. Adachi, *Angew. Chem., Int. Ed.*, 2017, **56**, 1571–1575.
27 Z. Yang, X. Ge, W. Li, Z. Mao, X. Chen, C. Xu, F. Long Gu, Y. Zhang, J. Zhao and Z. Chi, *Chem. Eng. J.*, 2022, **442**, 136219.
28 A. J. Gillett, A. Pershin, R. Pandya, S. Feldmann, A. J. Sneyd, A. M. Alvertis, E. W. Evans, T. H. Thomas, L.-S. Cui, B. H. Drummond, G. D. Scholes, Y. Olivier, A. Rao, R. H. Friend and D. Beljonne, *Nat. Mater.*, 2022, **21**, 1150–1157.
29 A. Huang, Q. Li and Z. Li, *Chin. J. Chem.*, 2022, **40**, 2356–2370.
30 Q. Li and Z. Li, *Acc. Chem. Res.*, 2020, **53**, 962–973.
31 T. Lu and F. Chen, *J. Comput. Chem.*, 2012, **33**, 580–592.
32 W. Wei, Z. Yang, X. Chen, T. Liu, Z. Mao, J. Zhao and Z. Chi, *J. Mater. Chem. C*, 2020, **8**, 3663–3668.
33 J. Zhang, L. Hu, K. Zhang, J. Liu, X. Li, H. Wang, Z. Wang, H. H. Y. Sung, I. D. Williams, Z. Zeng, J. W. Y. Lam, H. Zhang and B. Z. Tang, *J. Am. Chem. Soc.*, 2021, **143**, 9565–9574.
34 T. Hua, Y.-C. Liu, C.-W. Huang, N. Li, C. Zhou, Z. Huang, X. Cao, C.-C. Wu and C. Yang, *Chem. Eng. J.*, 2022, **433**, 133598.